nature astronomy

Article

https://doi.org/10.1038/s41550-022-01815-8

Rapid formation of exoplanetesimals revealed by white dwarfs

Received: 31 January 2022

Accepted: 26 September 2022

Published online: 14 November 2022

Check for updates

Amy Bonsor [1] ✉, Tim Lichtenberg [2,3,6], Joanna Drążkowska [4,5,6] & Andrew M. Buchan [1,6]

The timing of formation of the first planetesimals determines the mode of planetary accretion and their geophysical and compositional evolution. Astronomical observations of circumstellar disks and Solar System geochronology provide evidence for planetesimal formation during molecular cloud collapse, much earlier than previously estimated. Here we present distinct observational evidence from white dwarf planetary systems for planetesimal formation occurring during the first few hundred thousand years after cloud collapse in exoplanetary systems. A substantial fraction of white dwarfs have accreted planetary material rich in iron core or mantle material. For the exo-asteroids accreted by white dwarfs to form iron cores, substantial heating is required. By simulating planetesimal evolution and collisional evolution, we show that the most likely heat source is short-lived radioactive nuclides such as ^{26}Al (which has a half-life of ~0.7 Myr). Core-rich materials in the atmospheres of white dwarfs, therefore, provide independent evidence for rapid planetesimal formation, concurrent with star formation.

The timing and locations of planetesimal formation are crucial to our understanding of planet formation. If we are to form larger planets—gas giants or terrestrial planets—we must first form their building blocks: planetesimals. The meteorite record provides strong evidence that planetesimal formation in the Solar System spanned a wide range of ages, with magmatic iron meteorites dating to <1 Myr after the formation of Ca–Al-rich meteoritic inclusions (CAIs, the oldest known solids formed in the Solar System)[1,2], whereas carbonaceous chondrite meteorites record formation times extending to ~5 Myr after CAIs[3]. The key question for understanding the growth mechanism of planets such as Jupiter is whether planetesimals form sufficiently early to allow time for the accretion of larger protoplanets before the end of the circumstellar disk, the lifetimes of which are typically several million years[4]. Without knowledge of the timing of CAI formation, it is difficult to pin down whether planetesimal formation started in the Solar System during the collapse phase, traced observationally by Class 0/I disks, while the protostar is still accreting from the surrounding molecular cloud, or later, in Class II disks that are spatially isolated from their star-forming environments. Traditional planet formation models start with fully fledged Class II disks, assuming that all the solids are in the form of dust and that the dust evolution only starts at the beginning of the Class II phase. Observationally, Class II disks do not contain sufficient material as dust to form the observed population of exoplanets[5,6]. Observed substructures in very young circumstellar disks[7,8] may indicate the presence of over-densities where planet formation may already be underway during the Class 0/I stage[9,10], although these structures can also be explained by disk instabilities or condensation fronts[11,12]. Probing these disks with the Atacama Large Millimeter/submillimeter Array (ALMA) reveals the mass in millimetre/submillimetre grains (dust) as probed by its thermal emission, but planetesimals and larger protoplanets are invisible at ALMA wavelengths. Thus, the main observational way to probe the growth of planetesimals is to search for trends in dust depletion with disk stage, which are complicated by correlations between disk structure, size and disk stage, as well as observational biases in

[1]Institute of Astronomy, University of Cambridge, Cambridge, UK. [2]Atmospheric, Oceanic and Planetary Physics, Department of Physics, University of Oxford, Oxford, UK. [3]Kapteyn Astronomical Institute, University of Groningen, Groningen, the Netherlands. [4]University Observatory, Faculty of Physics, Ludwig-Maximilians-Universität München, Munich, Germany. [5]Max Planck Institute for Solar System Research, Göttingen, Germany. [6]These authors contributed equally: Tim Lichtenberg, Joanna Drążkowska, Andrew M. Buchan. ✉e-mail: abonsor@ast.cam.ac.uk

the disk and exoplanet populations[13,14]. Further evidence regarding the timing of planetesimal formation is therefore required to test the main channels and timescales of planetary growth.

In this work we present distinct observational evidence that planetesimal formation commenced early in a notable fraction of exoplanetary systems. This evidence comes from white dwarfs that have accreted planetary material. Fragments of planetary bodies from a surviving outer planetary system show up in the spectra of an otherwise clean (hydrogen/helium only) white dwarf[15,16]. From these observations, the composition, notably ratios of key elements such as Si, Mg, Fe, O, Ca, C, Cr or Ni in the planetary material, can be found. Elements heavier than helium should sink out of sight on timescales of days to millions of years, depending on the white dwarf temperature, surface gravity and atmospheric composition[17,18]. Thus, the observed material must have arrived recently. Planetary material is found in a large proportion of white dwarfs (30–50%; refs. [19,20]) with observations able to detect relatively small amounts of material (equivalent to kilometre-sized asteroids). For most white dwarfs, these observed abundances are consistent with the accretion of primitive rocky material, but for some white dwarfs there is an over- or underabundance of core affine (siderophile) species such as Fe, Cr and Ni relative to mantle affine (lithophile) species, such as Mg and Si, which is best explained by metal–silicate partitioning that occurs during the formation of an iron core[21–23]. These white dwarfs have accreted a fragment of the metal core or silicate mantle of a chemically differentiated planetary body[15].

Observations show that a substantial fraction of white dwarfs with planetary material in their atmospheres have accreted core- or mantle-rich material. As a conservative estimate, in a sample of more than two hundred white dwarfs (based primarily on Ca, Fe and Mg abundances), 4% are best explained (to >3 σ) by the accretion of core-rich material (Sample One; see 'Sample One' in the Methods). When more elements are detected, more information regarding the planetary material can be deduced. In the 54 white dwarfs with more than five elements detected considered here (Sample Two; see 'Sample Two' in the Methods), 7% were best explained (to >3 σ) by a model that invoked core–mantle differentiation[24] (note, however, that this sample was not selected in a uniform manner). The models used[24–26] placed stringent conditions on invoking core–mantle differentiation, took into account the abundances of all elements observed in each system and accounted for relative sinking, as well as volatile depletion and potential variations in the initial composition of the planet-forming material (see 'Models to explain the abundances observed in the atmospheres of white dwarfs' in the Methods). Only fragments with extremely core- or mantle-rich compositions would be identified, although we note here that additional processes such as impact melting (the suggested origin of low Ca/Fe ratios in CB chondrites[27]) are not included in the current models. The Ca/Fe ratios of the planetary material accreted by the 237 white dwarfs in both samples considered are shown in Fig. 1 as a function of white dwarf temperature, with the large circles indicating those objects with a >3 σ requirement for core-rich material, noting that the model does not identify many mantle-rich fragments (to >3 σ) due to a degeneracy between mantle-rich compositions and the depletion of moderately volatile elements.

The segregation of material between the iron-rich core and silicate mantle requires large-scale melting. If the white dwarfs accreted exo-asteroids, the most likely source of energy to fuel the large-scale melting is the decay of short-lived radioactive nuclides[28]. As seen in the Solar System[29], ^{26}Al fuels large-scale melting, with alternate species such as ^{60}Fe largely absent from the solar disk[30]. Here we show that it is unlikely that the white dwarfs accrete minor planets or the collision fragments of minor planets, where large-scale melting could have been fuelled by gravitational potential energy. ^{26}Al has a half-life of 0.717 Myr and its heating potential dwindles rapidly after ~1–2 half-lives. For planetesimals to contain sufficient ^{26}Al, they must form early, within the first million years of the evolution of the planetary system, when sufficient ^{26}Al for melting and large-scale differentiation is still present.

The distribution of short-lived radioactive nuclides across exoplanetary systems is unknown[31], with end-member inferences ranging from a small fraction of exoplanetary systems (a few percent; for example ref. [32]) to a notable fraction, potentially the majority of planetary systems (for example, ref. [33]) that feature Solar System-like abundances. Most works, however, suggest that few systems have substantially higher abundances of ^{26}Al than the Solar System[34–37], which is supported by observational evidence from individual star-forming regions[38,39]. Depending on when planetesimal formation occurs, this means that for some exoplanetary systems with high initial budgets of short-lived radioactive nuclides, a large fraction of planetesimals will form an iron core. For other exoplanetary systems with lower levels of enrichment only the small fraction of planetesimals that form early segregate to a differentiated mantle–core structure. Figure 2 illustrates this point, by showing the fraction of planetesimals likely to pollute a white dwarf (chosen to be between 50 and 300 km in diameter, approximately the birth size range produced by the streaming instability) that contain sufficient ^{26}Al to form an iron core as a function of the time at which they formed and the initial abundance of ^{26}Al in the system. This was calculated on the basis of the bodies reaching a mean internal temperature above which planetesimals can experience core–mantle differentiation by percolation of metal sulfide liquids using the models of ref. [40] and assuming a size distribution in planetesimals of $n(D)\mathrm{d}D \propto D^{-7/2}\mathrm{d}D$, where D is planetesimal diameter and n is the number of planetesimals per diameter, dD. Almost all planetesimals that form earlier than ~1 Myr form an iron core, whereas almost no bodies that form later than a few million years contain sufficient ^{26}Al to lead to large-scale melting. Even at five times higher abundances of ^{26}Al than solar, only a few bodies that form later than 2 Myr can form iron cores. Varying the initial size distribution and upper/lower bounds of the planetesimal population within plausible limits only marginally affected these overall conclusions.

Thus, if ^{26}Al fuels the large-scale melting, the observations of core- or mantle-rich material accreted by white dwarfs requires the early formation of planetesimals in exoplanetary systems, most likely within the first million years after the injection of ^{26}Al. With the injection of ^{26}Al at (or before) the start of the collapse of the molecular cloud[31,36,38,39], the white dwarf observations thus provide evidence that planetesimal formation occurred during the Class 0/I phase. A schematic illustrating the proposed scenario is shown in Fig. 3. Planetesimals that form early in systems with a sufficient budget of short-lived radioactive nuclides will undergo large-scale melting and form an iron core, as occurred for the parent bodies of iron meteorites in our Solar System. Leftover planetesimals not incorporated into planets form collisional belts, as shown by observations of debris disks[41]. Violent collisions can produce core- or mantle-rich fragments[42,43]. These fragments evolve in planetesimal belts. Belts exterior to a few astronomical units survive dramatic phases of evolution as their host stars become giants and lose their outer envelopes to start the white dwarf cooling phase. Scattering by planets, or other dynamical instabilities following stellar mass loss, can lead to some of these fragments being accreted by white dwarfs[44], where their core- or mantle-rich compositions show up in the atmosphere. Those planetary bodies that formed after ^{26}Al decayed undergo the same collisional evolution, scattering and accretion, but show up as primitive compositions in the atmosphere of the white dwarf. Thus, if the parents of the white dwarf pollutants are asteroids, the presence of core or mantle material is evidence for their formation within the first few hundred thousand years of cloud collapse.

Alternatively, as indicated by the dotted lines on Fig. 3, planetary bodies larger than about 1,400 km in diameter may form an iron core without the need for ^{26}Al. For such large bodies sufficient gravitational potential energy is available during formation to lead to large-scale melting[45] (see 'Gravitational potential energy as a driver of core–mantle differentiation' in the Methods). Moons or even terrestrial planets

https://doi.org/10.1038/s41550-022-01815-8

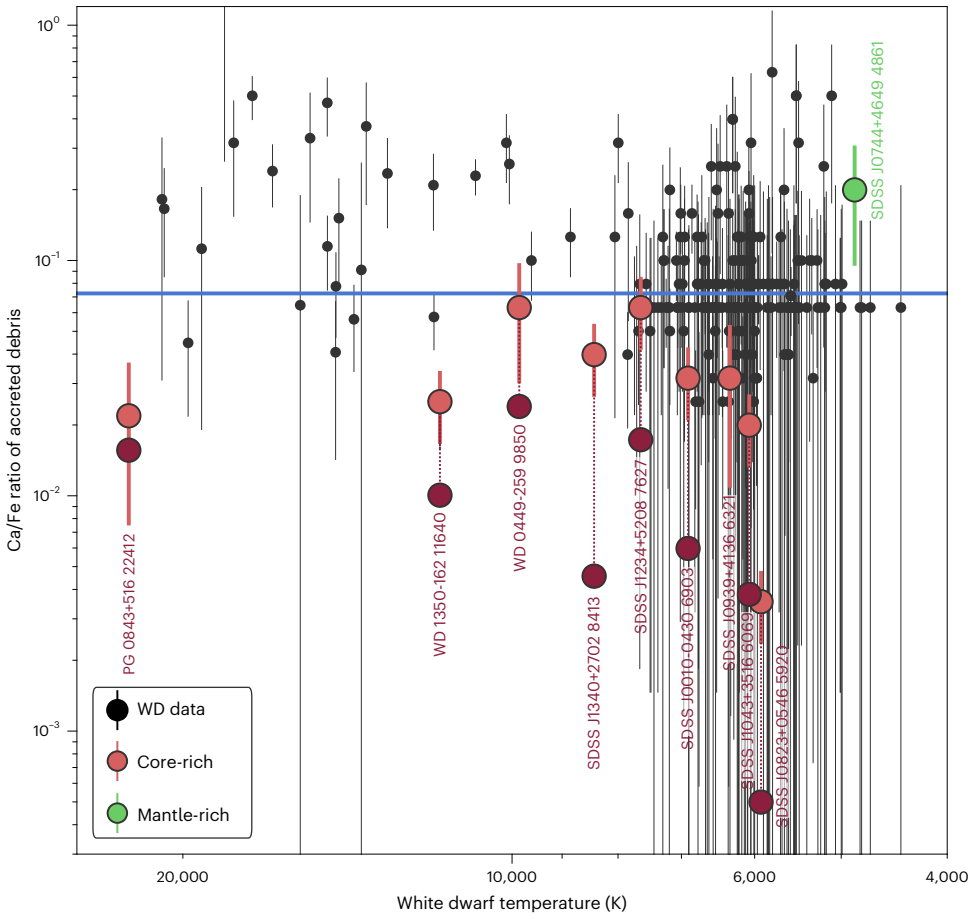

Fig. 1 | Enrichment in Fe, Ni and Cr relative to Ca, Mg and Si of planetary materials accreted by white dwarfs suggests the accretion of core- or mantle-rich material. The Ca/Fe ratios observed in a sample of 237 white dwarfs are shown with the associated 1 σ errors as a function of white dwarf temperature. The large red circles indicate the eight white dwarfs where a model in which core-rich material is accreted explains the observed abundances of all elements to >3 σ above a primitive model. In some cases the observed Ca/Fe is higher than the Ca/Fe in the accreted debris due to relative sinking, in which case the corrected abundances in the accreted material are plotted in dark red. SDSS J0744+4649 (shown in green) has Ca/Fe = 0.2 (ref. [63]) and high Na, potentially related to the accretion of material from planetary lithosphere[26]. Models from refs. [24–26]. The blue line indicates the solar Ca/Fe ratio.

undergo magma ocean phases and form iron cores due to this gravitational potential energy, but are rare (by number) relative to asteroids. Although dynamical mechanisms exist for the liberation of exomoons or the direct scattering of planets onto white dwarfs, such events seldom occur[46,47]. This is in stark contrast to the ubiquitous nature of the white dwarf pollution, with 30–50% of white dwarfs having planetary material in their atmospheres[19,20], pointing towards the accretion of moons/planets as an unlikely pathway for most pollution of white dwarfs. Nor are the core-rich systems outliers with higher than average accretion rates: the observed masses and inferred accretion rates for all but a handful of cool white dwarfs are asteroidal masses (or smaller)[48]. To accrete an Earth mass ($M_\oplus$) of material, accretion would need to be moderated at low accretion rates and continue on billion-year (or longer) timescales, as there are no observed accretion rates higher than ~10^{11} g s^{-1} (ref. [49]).

Theoretically, the largest planetary bodies within a planetesimal belt could form iron cores without the need for ^{26}Al. The existence of such large bodies within exoplanetesimal belts is debated due to the rapid decrease in the brightness of disks with time, which would not occur if collisions between large bodies were replenishing the small dust[50]. If a population of Pluto-sized bodies (Plutos) exists, their catastrophic collisions could dominate the mass budget of massive, close-in (fewer than a few astronomical units) planetesimal belts (see 'Collisional evolution of planetesimal belts' in the Methods; ref. [51]). In this scenario, most small planetary bodies are the collision fragments of Plutos. Thus, the 10–100 km asteroids polluting white dwarfs would probably show up with core- or mantle-rich compositions. The fraction of 30 km planetesimals that are fragments of Plutos (D > 1,400 km) is shown in Fig. 4a as a function of time. On timescales shorter than 10% of the collision lifetime (0.1 t_c, D = 1,400 km; equation (16)), fewer than 1% of the 30 km diameter planetesimals plausibly polluting white dwarfs would be collision fragments of core–mantle differentiated, D_* = 1,400 km, planetesimals. The proposed scenario can thus only occur in planetesimal belts where collisional evolution has proceeded for longer than t_c of Plutos. Figure 4b shows that only very massive, close-in planetesimal belts have a sufficiently short t_c for Plutos, approximately 1% of planetesimal belts, given the distribution of planetesimal belt properties that fits current observational samples[52]. Moreover, only a small fraction (on the order of 10%) of planetesimals in such systems would have compositions sufficiently core- or mantle-rich to be detected.

The white dwarf observations suggest that enrichment by ^{26}Al is common across exoplanetary systems. Large-scale melting fuelled by gravitational potential energy in Plutos or larger bodies is only likely to account for a tiny (<0.1%) fraction of white dwarf pollutants. Apart from the direct consequences for core–mantle differentiation, the common enrichment of exoplanetary systems by ^{26}Al has far-reaching

https://doi.org/10.1038/s41550-022-01815-8

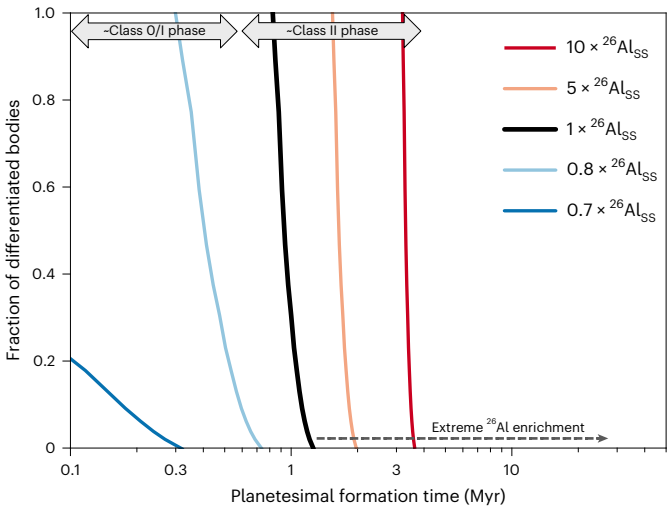

Fig. 2 | Almost all planetesimals that undergo core–mantle differentiation form within the Class 0/I collapse phase in exoplanetary systems with plausible levels of ^{26}Al enrichment. The fraction of planetary bodies likely to pollute white dwarfs (50–300 km in diameter) with sufficient ^{26}Al to form an iron core[40] is shown as a function of the time at which they formed. A size distribution of $n(D)\mathrm{d}D \propto D^{-7/2}\mathrm{d}D$ is assumed, and a range of ^{26}Al budgets above and below Solar System levels ($^{26}Al_{SS} = 5.25 \times 10^{-5}\ ^{27}Al_{SS}$) are shown. Few planetary systems have abundances notably above solar[31,34–39].

implications for the volatile budgets of rocky planets acquired during formation. Planetary bodies that form outside ice-lines lose their volatiles due to heating from ^{26}Al, introducing a disconnect between ice-lines and the volatile content of planets[40,53]. As the abundance and fractionation of highly volatile elements on rocky planets is key to their long-term climate[54], our findings highlight the influence of short-lived radioactive nuclides on the surface conditions and frequency of potentially temperate, Earth-like exoplanets. The need for enhanced abundances of ^{26}Al to explain core- or mantle-rich white dwarf spectra provides distinct evidence for the early formation of planetesimals in exoplanetary systems contemporaneously with star formation. Rapid planetesimal formation offers an explanation for the difference in mass budgets between Class 0, I and II disks[6]. Our findings point to the growth of large, >10-km-sized planetesimals, potentially even planetary cores, rather than just the coagulation of pebbles. The earlier planetary cores form, the more likely they are to grow to the pebble isolation mass and the more likely giant planet formation is to occur early on[55], which can provide an explanation for substructures commonly observed with ALMA. A new picture is emerging of star and planet formation starting concurrently, with large planetary bodies forming and geophysically evolving during the collapse of the planet-forming disk, which is traditionally associated with Class 0/I systems.

Methods

To determine how frequently the planetary bodies accreted by white dwarfs underwent large-scale melting and differentiated internally, core- and mantle-rich compositions were identified by analysing the abundances observed in two distinct samples of polluted white dwarfs. The first was selected for outcome (more than five elements detected) and contained predominantly white dwarfs with high-quality data, whereas the second contained only DZs, observed and analysed in the same manner, based on their Sloan Digital Sky Survey (SDSS) spectra. The following sections describe the models used to explain the observed abundances and the two white dwarf samples considered here.

Models used to explain the abundances observed in the atmospheres of white dwarfs

The white dwarfs considered here all have spectra in the optical and/or UV, with abundances for a number of metals species in the hydrogen or helium atmosphere previously presented in the literature. The most likely explanation for the observed abundances was found using Bayesian models presented in refs. [24–26] (https://github.com/andrewmbuchan4/PyllutedWD_Public). The results for most white dwarfs considered were presented previously in refs. [24,26], with those analysed specifically for this Article detailed in Supplementary Table 1. These models considered all the elements that have been detected, alongside upper limits where available. These models did not take into account S, Sc, Cu, Co, V, P, Mn, Ga, Ge, K, Li or Be. The potential that the observed abundances were altered from those in the accreted planetary material due to relative sinking was considered. A range of initial conditions for the planetary material were considered, with the compositions of nearby stars[56] used as a proxy for this range. The abundances in the planetary material can be altered due to loss of volatiles, which for the simplest scenario is just the loss of water to make rocky asteroids. However, all elements, including moderate volatiles such as Na, were considered and this loss of volatiles was modelled as the incomplete condensation of the nebula gas in chemical equilibrium. The white dwarf was then allowed to accrete a fragment of a larger planetary body with the core mass fraction being a free parameter. In other words, the white dwarf could accrete a chunk of the iron core (core mass fraction = 1) or a chunk of silicate mantle (core mass fraction = 0), or a chunk of predominantly core material with some mantle remaining (for example core mass fraction = 0.9) and so on. The compositions of the core and mantle material were allowed to vary depending on the pressure and oxygen fugacity conditions under which the planetary body formed its iron core, using metal–silicate partitioning parameterized according to refs. [57–62].

White dwarf observations

Sample One. A sample of 202 cool white dwarfs with only metal features (DZ) were selected from their SDSS spectra with detections of at least Mg, Fe and Ca from refs. [63,64]. We note here that magnetic or unresolved binary white dwarfs were not included in the sample and that updated abundances from refs. [26,65] were used. The spectra had relatively low S/N compared with Sample Two targets and thus fewer elements were detected and the uncertainties were larger. White dwarfs in this sample for which more than five elements were detected were also included in Sample Two. These white dwarfs were predominantly selected due to their colours in SDSS (u–g) (g–r) space, where the large absorption features due to the presence of metals in these white dwarf spectra move the white dwarfs from above the main sequence to below the main sequence. This selection function may thus have biased the sample towards white dwarfs with high Ca abundances; however, the requirement that Fe and Mg must also be detected meant that the distribution of Ca/Fe in the sample was only slightly skewed to high Ca/Fe (ref. [66]). This sample of white dwarfs was analysed in ref. [26] in detail; crucially, it was found that mantle-rich fragments are harder to identify due to a degeneracy with sinking and volatile depletion. Ref. [26] identified 7/202 (4%) white dwarfs where the accretion of core-rich material is required to >3 σ over the accretion of primitive material. We note here that ref. [26] incorrectly stated that eight white dwarfs were best explained by the accretion of core-rich material, when eight white dwarfs were best explained by the accretion of core–mantle differentiated material. One object (SDSS J0744+4649) was identified where the Ca, Fe and Mg abundances suggested an enhancement of Ca and Mg relative to Fe, as seen in planetary mantles, with the enhanced Na indicating that this cannot be due to volatile depletion[26]. The full details of the sample are presented in the supplementary information of ref. [26].

https://doi.org/10.1038/s41550-022-01815-8

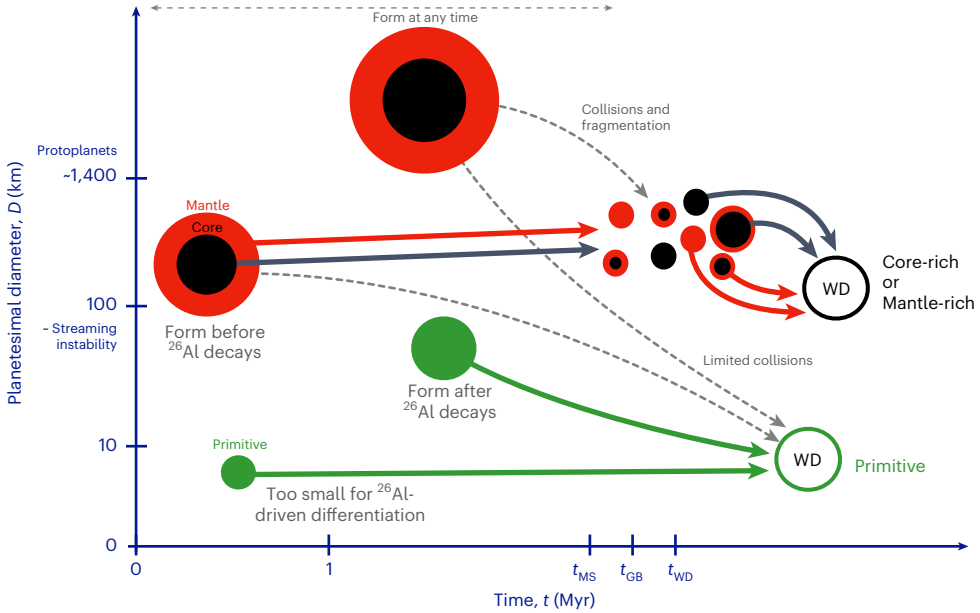

Fig. 3 | The core- or mantle-rich materials in the atmospheres of white dwarfs are the collision fragments of planetesimals that formed earlier than ~1 Myr, when large-scale melting was fuelled by the decay of ^{26}Al. Alternatively, in the most massive, close-in, highly excited planetesimal belts, catastrophic collisions between Pluto-sized bodies (D > 1,400 km) could supply most smaller planetesimals. Gravitational potential energy during accretion can fuel large-scale melting and core formation in these large bodies, such that almost all planetary bodies in the belt are the collision fragments of bodies with differentiated cores (black) and mantles (red). t_{MS}, t_{GB} and t_{WD} are the star's main sequence and giant branch lifetimes and the start of the white dwarf (WD) phase.

Sample Two. Sample Two comprised 54 white dwarfs selected from the literature with abundances of more than five elements, including Fe. These white dwarfs tended to be the most highly polluted, the brightest stars and the most studied objects; 19 of these white dwarfs were also included in Sample One. Most have high-resolution spectra, potentially from multiple instruments. By necessity, however, the selection of the sample was observationally biased, with many observations tending to target those objects that were easiest to measure. The atmospheric abundances were analysed using the model presented in ref. [24], which updates the models of ref. [26] by modelling core–mantle differentiation without any assumption of Earth-like material. Although the most likely explanation (strongest evidence from Bayesian models) for the observed abundances includes core–mantle differentiation for one-third of the sample (19/54), the abundances were consistent (within the errors) for most white dwarfs with the accretion of primitive material—the abundances of which were only altered by volatile loss, sinking in the white dwarf atmosphere and the potential small variation in the composition of the initial planet-forming material. For another three systems (NLTT43806, LHS 2534 and SDSS J0744+4649), previous work suggested the accretion of crust-rich material to explain the abundances[26,67,68]. The model used here did not account for crustal differentiation.

In identifying those white dwarfs that potentially accreted core- or mantle-rich fragments of larger planetary bodies, the relatively large uncertainties on the atmospheric abundances (as well as the unknown time since accretion started, which determines the relative sinking of elements) play an important role. In many cases the Bayesian models found the strongest evidence for a model that invoked core-rich material. This is indicated by the Bayes factor, which ref. [26] and ref. [24] convert to a σ significance[69] using equation (10) of ref. [26]. We focused here on those systems where the statistical significance to which a model that includes core–mantle differentiation over and above a model that invokes only sinking to explain the observed abundances, $\sigma_{diff} > 3$, although noting that core-rich material may well be the true explanation for systems with $\sigma_{diff} < 3$. Core–mantle differentiation is required (>3 σ) to explain the abundances in 4/54 (7%) of systems (PG 0843+516, SDSS J1043+3516, WD 0449-259 and WD 1350-162), but note that in Sample One, for the systems SDSS J0939+4136 and SDSS J1234+5208 the Earth-like differentiation models of ref. [26] increased the significance to which core–mantle differentiation was invoked from slightly below to over 3. Including the three crust-rich systems, at least 7/54 (13%) underwent large-scale melting and plausibly a substantially higher fraction. The sample is slightly different from that presented in ref. [24], now including 19 additional objects with more than 5 elements detected, but did not include Ni, Cr or Si, as required by ref. [24], while not including objects with <5 elements detected. However, the analysis is identical to that performed by ref. [24], which updated the model of ref. [26] to allow for core–mantle differentiation in systems with arbitrary (rather than Earth-like) compositions.

The full list of white dwarfs in the sample is presented in Supplementary Table 1, the atmospheric abundances used in this work are listed in Supplementary Table 2 and the most likely model parameters, as determined by the Bayesian models, are presented in Supplementary Table 3. We note here that the model has been updated since ref. [25] to include updated sinking timescales, as well as a stricter criterion for where the accretion of core–mantle differentiated material is required to explain the observed abundances. We note that a discrepancy exists between abundances determined from UV and optical data (see ref. [70] for more details). For a number of white dwarfs where conflicting abundances exist, a consistent set of abundances from the UV was used and is noted in Supplementary Table 2.

Gravitational potential energy as a driver of core–mantle differentiation

During the formation of the largest planetesimals, or indeed moons or terrestrial planets, there is sufficient gravitational potential energy available that, when converted to heat, large-scale melting can occur. To estimate how large a planetesimal must be for there to be sufficient gravitational potential energy, the energy deposited in a body by the accretion of smaller objects, per unit mass, is considered to be $E \approx \frac{h}{2}(v_{esc}^2 + v_{rel}^2)$, where h is the fraction of the energy deposited as heat, rather than reradiated, v_{esc} is the escape velocity of particles from

https://doi.org/10.1038/s41550-022-01815-8

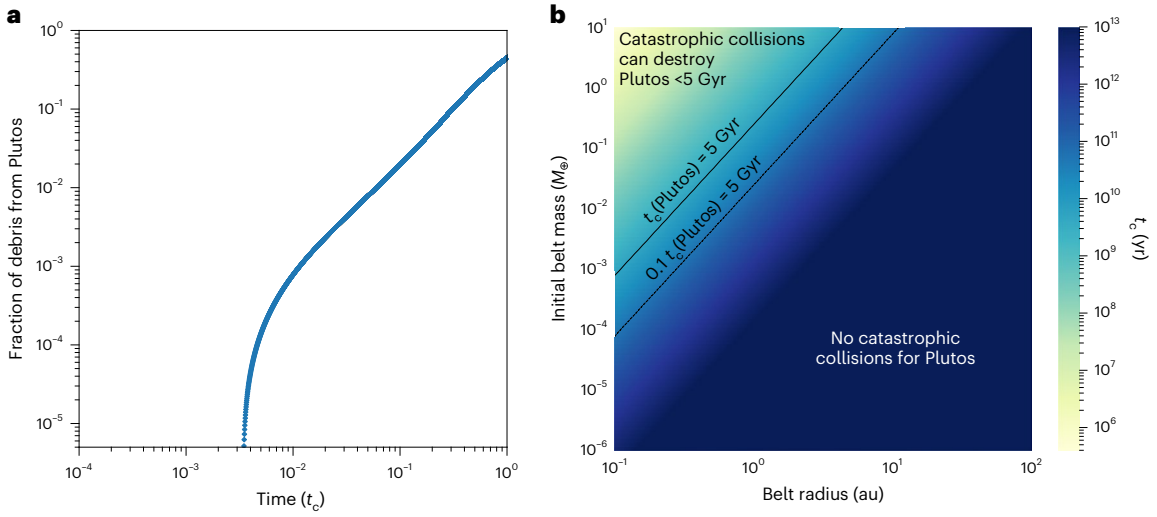

Fig. 4 | Plutos can be the source of core-rich planetesimal debris only in rare (<1%) white dwarf systems with massive, close-in planetesimal belts. a, The fraction of 30-km-diameter debris that comprises fragments of core–mantle differentiated Plutos (in units of t_c, equation (16)) is shown for a belt at 1 au with average particle eccentricity $\langle e \rangle = 0.1$ and initial mass of 100 $M_\oplus$ in particles with sizes between 100 μm and 5,000 km. **b**, Approximation of collision lifetime, t_c (colour scale) as a function of the initial mass in the planetesimal belt in bodies between 100 μm and 1,400 km in diameter and the belt radius (equation (16)). A collision lifetime t_c of 5 Gyr is shown by the solid black line and 0.1 t_c by the dashed black line. Less than 1% of debris disks, those with very massive, close-in planetesimal belts that lie in the top-left corner above the solid line, will have catastrophic collisions of Plutos ($D > 1{,}400$ km bodies) supplying material to the smaller planetesimals that might pollute white dwarfs based on typical properties of observed debris disks. This is too low to explain the 4% (Sample One, see 'Sample One' in the Methods) to >13% (Sample Two, see 'Sample Two' in the Methods) of white dwarf pollutants that accreted fragments of core–mantle differentiated bodies.

a planetesimal of mass M and radius R, and v_{rel} is the relative velocity between the particles and the growing planetesimal, following ref. [45]. Given that the relative velocity of most particles is approximately the escape velocity, this becomes $E \approx \frac{hGM^2}{R}$ (where G is the gravitational constant), which for spherical planetesimals of uniform density is approximately $E = \frac{hG\rho R^2 4\pi}{3}$, where ρ is the density of the planetesimal. The energy required to raise the temperature from typical temperatures at the mid-plane of protoplanetary disks (around 700 K) to the temperatures required for large-scale melting (~1,200 K), assuming the specific heat capacity of the body is around that for silicates ($C_p = 800$ J kg^{-1} K^{-1}), is 4×10^5 J kg^{-1} (ref. [45]). Using a conservative $h = 0.8$ and a density of 3 g cm^{-3} a planetesimal of radius >700 km (>1,400 km diameter) can become differentiated by gravitational energy alone.

Collisional evolution of planetesimal belts

One route to get core- or mantle-rich pollutants into the atmosphere of white dwarfs is to scatter in asteroids (10–300 km in size) that are themselves fragments of Plutos ($D > 1{,}400$ km), bodies large enough to form an iron core without the need for heating from short-lived radioactive nuclides (see 'Gravitational potential energy as a driver of core–mantle differentiation'). These bodies can form at any time (Fig. 3). If there are sufficient collisions in a planetesimal belt, the Plutos can reach collisional equilibrium and fragments of these large bodies will feed the population of smaller bodies in the belt. We present models for the collisional evolution of planetesimal belts that determine the fraction of asteroids ($D = 10$–300 km) that are fragments of Plutos ($D > 1{,}400$ km) as a function of time. In these systems, core- or mantle-rich fragments could be accreted by white dwarfs from planetesimals that formed at any epoch. We found that this is a rare pathway to white dwarf pollution. The simulations show that before smaller bodies are likely to be fragments of a larger body of a given size, D_{eq}, those bodies must reach (or almost) reach collisional equilibrium—or in other words, a time $t_c(D_{eq})$ (equation (16)) must pass. As it takes a long time for Plutos to reach collisional equilibrium, this only occurs in the most massive, close-in planetesimal belts, of which too few exist for them to be the likely source of many white dwarf pollutants.

Collision model. The model traced the collisional evolution of a planetesimal belt with time. The mass in the belt was split into logarithmically spaced bins and the origin of the mass in each size bin was traced as a function of time. In other words, the aim was to answer the question of whether most white dwarf pollutants (of size, for example, 30 km) are collision fragments of larger bodies, in particular bodies larger than 1,400 km.

The model for collisional evolution was based on ref. [71], presented in detail in A.B. et al. (manuscript in preparation). Here we considered solids only and catastrophic collisions only. We considered the belt to be a single annulus that contains particles from size M_{min} to M_{max}, or equivalently from diameter D_{min} to D_{max}, where spherical particles of constant density were assumed, such that particles in the kth bin of diameter, D_k, have a mass $M_k = \frac{\pi D_k^3}{6}$ with a size distribution:

$$n(M)\,\mathrm{d}M \propto M^{-\alpha}\mathrm{d}M \quad (1)$$

We assumed a standard infinite collisional cascade[51,72], with a power-law index of $\alpha = 0.83$, or equivalently for diameter $q = 3.5 = 3\alpha + 1$. The size distribution was split into bins of equal width in log space (δ), labelled by their mass, M_k. The spacing δ was assumed to be small, such that $\frac{M_{k+1}}{M_k} = 1 - \delta$. At every time step, we calculated the rate at which each bin gained and lost mass. We assigned a fractional origin of material in each bin from every other larger mass bin in the system. At each time step, this fractional origin of material was updated, taking into account the origin of the mass gained and lost in each mass bin, as well as the mass that stayed in this bin from previous time steps.

To trace the collisional evolution of the material between size bins, a threshold was defined, such that the smallest particle that can destroy a body of size M_k is given by:

$$M_k^c = \left(\frac{2Q_D^*}{v_{rel}^2}\right) M_k \quad (2)$$

where v_{rel} is the relative velocity in collisions and Q_D^* is the specific incident energy required to cause a catastrophic collision, or the dispersal threshold. The ratio of the smallest size that can destroy a body to its size is given by $X_c = \frac{M_k^c}{M_k}$. We assume a power-law form for the dispersal threshold, following work on collision outcomes in refs. [73,74], such that:

$$Q_D^* = Q_a(D)^{-a} + Q_b(D)^b, \quad (3)$$

where a and b are both positive constants related to the planetesimal's material and gravitational strength, respectively, and D is the planetesimal diameter in metres. Following ref. [71] we take $Q_a = 620\ \mathrm{J\ kg^{-1}}$, $a = 0.3$, $Q_b = 5.6 \times 10^{-3}\ \mathrm{J\ kg^{-1}}$ and $b = 1.5$. The rate of catastrophic collisions in the kth bin R_k^c is given by:

$$R_k^c = \Sigma_{i=1}^{i_{ck}} \frac{n_i}{4}(D_k + D_i)^2 P_{ik}, \quad (4)$$

where n_i is the number of colliders in the ith bin and P_{ik} is the intrinsic collision probability, $P_{ik} = \frac{\pi v_{rel}}{V}$, where V is the volume through which the planetesimals, of mass M_k are moving. i_{ck} refers to the smallest impactors that can cause catastrophic destruction, of mass M_k^c (equation (2)).

We consider that mass is conserved such that the total mass in solids in the k^{th} bin, $m_{s,k}$ is governed by the following equations:

$$\dot{m}_{s,k} = \dot{m}_{s,k}^{+c} - \dot{m}_{s,k}^{-c} \quad (5)$$

where $\dot{m}_{s,k}^{-c}$ is the rate at which the total mass in the k^{th} bin is lost to catastrophic collisions, given by:

$$\dot{m}_{s,k}^{-c} = m_{s,k} R_k^c, \quad (6)$$

and $\dot{m}_{s,k}^{+c}$ is the rate at which the mass in solids is gained from catastrophic collisions of larger bodies, given by:

$$\dot{m}_{s,k}^{+c} = \Sigma_{i=1}^{i_{mk}} F(k-i)\, \dot{m}_{s,i}^{-c}, \quad (7)$$

where $F(k-i)$ is the fraction of the mass leaving the ith bin from collisions that goes into the kth bin, or the redistribution function, which we assumed to be scale independent. We assumed that fragments produced in catastrophic collisions had a range of masses from the largest fragment, with $\frac{M_i}{2}$ labelled i_{lr}, to the smallest body considered, labelled i_{max}, which we assumed to be much smaller than $\frac{M_i}{2}$. Thus, the kth bin can only gain mass from catastrophic collisions between objects with a mass $2M_k$ or greater, labelled $i_{mk} = k - \frac{ln(2)}{\delta}$. The mass rate gained for solids in the kth bin was thus calculated by summing all of the contributions from the largest mass bin, $i = 1$, down to i_{mk}, which labels the bin of mass $2M_i$. We assumed that the scaling of the mass distribution of the fragments $\alpha > 1$ and that the logarithmic spacing between mass bins $\delta \ll 1$. This led to a redistribution function given by:

$$F_s(k-i) = (1-\delta)^{(k-i)(2-\alpha)} \delta (2-\alpha) 2^{(\alpha-2)}. \quad (8)$$

This is based on equation (20) of ref. [71], where δ is the spacing between mass bins and not radial bins, $\eta_{max} = 1/2$, such that $\delta = \delta'/3$ and $\alpha' = 3\alpha - 2$, where δ' and α' are the parameters used in ref. [71].

At each time step, we used equations (5), (6) and (7) to track the mass gained and lost. We also tracked $O_{k,i}$, which refers to the mass in the kth bin that originated from the ith bin. At every time step, of length Δ, each jth bin loses mass at $m_{s,j}^c R_j^c \Delta$, a fraction $O_{j,i}$ that originally came from the ith bin. To keep track of the evolution of mass that started the simulation in the ith bin, we calculated:

$$O_{k,i} = \frac{\left(O_{k,i} m_{s,k} - O_{k,i} m_{s,k} R_k^c \Delta + \Sigma_{j=1}^{j_{mk}} O_{j,i} F(k-j) m_{s,j} R_j^c \Delta\right)}{m_{s,k} - m_{s,k} R_k \Delta + \Sigma_{j=0}^{j_{mk}} F(k-j) m_{s,j} R_j^c \Delta}, \quad (9)$$

and keep track of the mass originating in the kth bin that remains in the kth bin, which is crucial for tracing the mass of material that has never been involved in collisions and thus, never changed bins:

$$O_{k,k} = \frac{O_{k,k} m_{s,k} - O_{k,k} m_{s,k} R_k^c \Delta}{m_{s,k} - m_{s,k} R_k \Delta + \Sigma_{j=0}^{j_{mk}} F(k-j) m_{s,j} R_j^c \Delta} \quad (10)$$

where the denominator is just the mass in the bin at the next time step. There should be no material in the bins with $i > i_{mk}$ and the sum of $\Sigma_{i=1}^{i_{max}} O_{k,i} = 1$ for conservation of mass. As each bin loses mass ($m_{s,k} R_k^c$) every time step, we assumed that a fraction $O_{k,i}$ was lost from the material in k originating from i.

Simulations

Individual planetesimal belts were simulated by distributing mass between size bins, according to an initial size distribution, with $\alpha = 3.5$ and logarithmic bins of width $\delta = 0.2$ (equation (1)). The mass in each size bin was iterated forwards in time according to equation (5). We fixed the belt width, dr at 0.5, the particle's density at $3 \times 10^3\ \mathrm{kg\ m^{-3}}$ and considered belts with initially 100 $M_\oplus$ of material at a radius of 1 au and with an initial particle eccentricity of 0.1. We considered particles with diameters between $D_{min} = 100\ \mu\mathrm{m}$ and 5,000 km (an arbitrary upper bound, which it will be shown did not influence the results). The bin width and time step were chosen to be sufficiently small that the mass lost and gained by the smallest particles in one time step remain a small fraction of the total mass in that bin, with $\delta_t = 10^6$ s.

The material in the belt was rapidly collisionally depleted. The smallest grains quickly reached collisional equilibrium, while the largest grains/planetesimals were unlikely to suffer collisions and retained their primordial size distribution. The left-hand panel of Supplementary Fig. 1 shows the size distribution of an example planetesimal belt at 1 au. The apparent wave in the size distribution results from the grain cutoff at a single size for the smallest grains, as discussed in (for example) refs. [71,75]. Those bodies for which t_c was less than the age of the system were collisionally depleted ($t_c(D) < t$), while larger bodies were not collisionally evolved. For older systems, larger and larger bodies entered collisional equilibrium.

If we considered a t_c of[76] (equation (7)):

$$t_{c(D)} = t_{per} \frac{r dr}{\sigma_{tot}} \frac{2I}{f(e,I)} \frac{1}{f_{cc}} \quad (11)$$

where t_{per} is the orbital period, $f(e, I)$ is the ratio of the relative velocity of collisions to the Keplerian velocity (v_{rel}/v_k), and e and I are the mean particle eccentricity and inclinations, σ_{tot} is the total cross-sectional area and f_{cc} is the fraction of the total cross-sectional area in the belt that is seen by planetesimals of size D as potentially causing a catastrophic collision. Following ref. [76], this can be written as:

$$f_{cc} = \left(\frac{D_{min}}{D}\right)^{3q-5} G(q, X_c), \quad (12)$$

where $G(q, X_c)$ is a function of both the size distribution (q) and the ratio of the smallest planetesimal (D_{cc}) that has enough energy to catastrophically destroy a planetesimal of size $_D$, $X_c = D_{cc}/D$. This can be calculated in terms of Q_D^*:

$$X_c = \left(\frac{2Q_D^*}{v_{rel}^2}\right)^{1/3}. \quad (13)$$

For a typical collisional cascade, $X_c \ll 1$, such that the function $G(q, X_c)$, for $q = 11/6$, can be approximated as $G(11/6, X_c) \approx 0.2X_c^{-2.5}$ for $X_c \ll 1$. σ_{tot} can be related to the total disk mass (M_{tot}):

$$\frac{\sigma_{tot}}{M_{tot}} = \frac{3}{4\rho}\frac{D_{min}^{5-3q}}{D_{max}^{6-3q}}\left(\frac{3q-6}{5-3q}\right) \quad (14)$$

Thus, leading to an expression for the collisional lifetime of a particle of diameter D:

$$t_c = t_{per}\frac{rdr}{\sigma_{tot}}\frac{2I}{f(e,I)}\frac{1}{f_{cc}} \quad (15)$$

$$= t_{per}\frac{rdr\,4\rho D}{3M_{tot}}\frac{2I}{G(q,X_c)f(e,I)}\left(\frac{3q-5}{6-3q}\right). \quad (16)$$

As time passes, larger and larger particles reach collisional equilibrium. The size particle that has just reached collisional equilibrium (D_{eq}) can be approximated by the size particle for whom the collisional lifetime is equal to the current time $t = t_c(D_{eq})$. In the regime where D is large ($D > 800$ m), Q_D^* (equation (3)) can be approximated as $Q_D^* \approx Q_b D^b$. Then D_{eq} is given by:

$$D_{eq} = (t/K)^{1/(1+5b/6)}, \quad (17)$$

where

$$K = t_{per}\frac{0.2rdr4\rho}{3M_{tot}}\frac{2I}{f(e,I)}\left(\frac{v_{rel^2}}{2Q_b}\right)^{5/6}.$$

We note here that this size is an approximation and that the absence of small grains leads to a size distribution that deviates from a perfect power law (see Supplementary Fig. 1).

The collisional cascade is fed by the largest bodies

The bodies that have just reached collisional equilibrium (D_{eq}) dominate the mass evolution of the belt[71]. Here we traced the origin of the material arriving in each size bin using equations (9) and (10), with the aim of investigating the extent to which the bodies that have just reached collisional equilibrium dominate the mass budget in small bodies. The smallest bodies are continuously lost from the collisional cascade, and thus, new material must replenish bodies of all sizes.

The right-hand panel of Supplementary Fig. 1 shows the fraction of the mass in the diameter bin centred on $D_k = 100$ m that originated from larger diameters. $D_k = 100$ m was chosen to represent any particles that are fully in collisional equilibrium and constantly being resupplied by collisions between larger bodies. The mass budget was indeed dominated by bodies of around D_{eq}, as shown by the vertical lines. D_{eq} as calculated by equation (17) is an approximation, not taking into account the wavy nature of the size distribution, and does not perfectly calculate the true maximum size in collisional equilibrium (see Supplementary Fig. 1), nor align perfectly with the maximum here, but the approximation is good to within a factor of a few.

Figure 4b shows the fraction of material in the smaller size grains that originated from grains larger than a certain size, 1,400 km, as a function of time, plotted in units of the collisional lifetime of these largest bodies ($t_c(D = 1{,}400$ km). As the bodies enter collisional equilibrium, they dominate the mass in smaller size bins, but the mass in small bodies (D_{in} from $D > 1{,}400$ km tends to one only on timescales longer than the collision timescale. The fraction of material from $D > 1{,}400$ km in 30 km planetesimals reaches 1% after $0.1t_c(D_*)$. This would apply to the fraction of planetesimals, $D > D_*$ in the bin labelled by $D_*/50$, where in this case $D_* = 1{,}400$ km.

The form of the right-hand panels of Supplementary Fig. 1 and Fig. 4 remains similar for different diameters, and we assert that within the validity of the approximation for t_c and accounting for small differences due to the wavy nature of the size distribution, the form of these figures is independent of the sizes D_* and D_{in}. Any differences result from the wavy nature of the size distribution and the approximations used in $t_c(D)$, whose validity change with diameter. The self-similar nature of the collisional cascade saves us from needing to run the collisional model for sufficiently long timescales that bodies of >1,400 km enter collisional equilibrium.

Frequency of Pluto-fed polluted white dwarfs

Although planetesimal belts sufficiently massive and sufficiently close-in that even the largest ($D > 1{,}400$ km) planetary bodies are collisionally evolving are rare, the aim of the following section is to assess whether they are sufficiently common to explain core(mantle)-rich compositions in some pollutants of white dwarfs. In this scenario, no ^{26}Al would be required to form an iron core.

Assuming that all planetesimal belts contain bodies larger than 1,400 km, the properties of those planetesimal belts in which large ($D > 1{,}400$ km) bodies would be collisionally evolving can be estimated by considering a typical lifetime for the planetary system. Many white dwarfs evolved from main sequence A stars, for which typical main sequence lifetimes are on the order of hundreds of million years. Belt radii expand by a factor of 2–3 during the white dwarf phase, following mass loss, so the majority of the collisional evolution occurs during the main sequence phase[77]. For solar-type stars, main sequence lifetimes can be as long as tens of billion years, but the age of the Universe stipulates that very few white dwarfs had main sequence lifetimes this long. Thus, we considered a conservative estimate on the timescale for which collisional evolution occurred of 5 Gyr. Using a typical distribution of planetesimal belts, fitted to observations of debris disks around main sequence A stars[52], with a distribution of initial belt radii of $n(r)dr \propto r^{\gamma}dr$, where $\gamma = -0.8$, between 3 and 200 au, the distribution of initial belt masses forms a log normal distribution of width 1.13 dex, centred on 10 $M_\oplus$ of width $M_\oplus$, we found that a few tenths of a per cent of belts have a collisional lifetime for particles of size 1,400 km of less than 5 Gyr. About a per cent of systems have 10% of the collisional lifetime of $D = 1{,}400$ km of less than 5 Gyr. Planetary systems in which such large bodies are catastrophically colliding are rare. Thus, planetary systems where 10–100 km planetesimals are likely to be the collision fragments of larger core–mantle differentiated Plutos are rare. Moreover, only a subset of collision fragments will have core or mantle compositions sufficiently extreme to be detected. If this fraction is on the order of 10% (see for example fig. 3 of ref. [66]), we anticipate that core- or mantle-rich compositions would show up in ≪0.05% of white dwarfs without the need for ^{26}Al. Thus, only a tiny fraction of white dwarf pollutants are likely to originate from large bodies, as this fraction is significantly lower than the fraction of white dwarf pollutants that seem to be core(mantle)-rich of at least 4% (see 'Sample One' and 'Sample Two').

The existence of large bodies in planetesimal belts has also been brought into question[50], and if such large bodies do exist, it is not clear whether they would have the same size distribution as the rest of the belt. However, it is plausible that in some planetary systems dynamical instabilities lead to high velocity collisions or excite collisions in planetesimals belts outside of the normal steady-state collisional evolution considered here.

Data availability

The data used to create Figs. 1–4 are available in the Supplementary Information; the white dwarf data (Sample Two) are provided in Supplementary Tables 1–3, while data for Sample One can be found in ref. [26]. Source data are provided with this paper.

Code availability

The code used to create Figs. 1–4 and the collisional evolution code is available at https://github.com/abonsor/collcascade and models for Fig. 2 are available at https://github.com/timlichtenberg/2stage_scripts_data.

References

1. Scherstén, A., Elliott, T., Hawkesworth, C., Russell, S. & Masarik, J. Hf–W evidence for rapid differentiation of iron meteorite parent bodies. *Earth Planet. Sci. Lett.* **241**, 530–542 (2006).
2. Kruijer, T. S. et al. Protracted core formation and rapid accretion of protoplanets. *Science* **344**, 1150–1154 (2014).
3. Kleine, T. et al. The non-carbonaceous-carbonaceous meteorite dichotomy. *Space Sci. Rev.* **216**, 55 (2020).
4. Fedele, D., van den Ancker, M. E., Henning, T., Jayawardhana, R. & Oliveira, J. M. Timescale of mass accretion in pre-main-sequence stars. *Astron. Astrophys.* **510**, A72 (2010).
5. Najita, J. R. & Kenyon, S. J. The mass budget of planet-forming discs: isolating the epoch of planetesimal formation. *Mon. Not. R. Astron. Soc.* **445**, 3315–3329 (2014).
6. Tychoniec, Ł. et al. Dust masses of young disks: constraining the initial solid reservoir for planet formation. *Astron. Astrophys.* **640**, A19 (2020).
7. Sheehan, P. D. & Eisner, J. A. Multiple gaps in the disk of the class I protostar GY 91. *Astrophys. J.* **857**, 18 (2018).
8. Segura-Cox, D. M. et al. Four annular structures in a protostellar disk less than 500,000 years old. *Nature* **586**, 228–231 (2020).
9. Stammler, S. M. et al. The DSHARP rings: evidence of ongoing planetesimal formation? *Astrophys. J. Lett.* **884**, L5 (2019).
10. Carrera, D., Simon, J. B., Li, R., Kretke, K. A. & Klahr, H. Protoplanetary disk rings as sites for planetesimal formation. *Astron. J.* **161**, 96 (2021).
11. Flock, M. et al. Gaps, rings, and non-axisymmetric structures in protoplanetary disks. From simulations to ALMA observations. *Astron. Astrophys.* **574**, A68 (2015).
12. Zhang, K., Blake, G. A. & Bergin, E. A. Evidence of fast pebble growth near condensation fronts in the HL Tau protoplanetary disk. *Astrophys. J. Lett.* **806**, L7 (2015).
13. van der Marel, N. & Mulders, G. D. A stellar mass dependence of structured disks: a possible link with exoplanet demographics. *Astron. J.* **162**, 28 (2021).
14. Mulders, G. D., Pascucci, I., Ciesla, F. J. & Fernandes, R. B. The mass budgets and spatial scales of exoplanet systems and protoplanetary disks. *Astrophys. J.* **920**, 66 (2021).
15. Jura, M. & Young, E. D. Extrasolar cosmochemistry. *Annu. Rev. Earth. Planet. Sci.* **42**, 45–67 (2014).
16. Farihi, J. Circumstellar debris and pollution at white dwarf stars. *N. Astron. Rev.* **71**, 9–34 (2016).
17. Fontaine, G. & Michaud, G. Diffusion time scales in white dwarfs. *Astrophys. J.* **231**, 826–840 (1979).
18. Koester, D. Accretion and diffusion in white dwarfs. New diffusion timescales and applications to GD 362 and G 29-38. *Astron. Astrophys.* **498**, 517–525 (2009).
19. Zuckerman, B., Melis, C., Klein, B., Koester, D. & Jura, M. Ancient planetary systems are orbiting a large fraction of white dwarf stars. *Astrophys. J.* **722**, 725–736 (2010).
20. Koester, D., Gänsicke, B. T. & Farihi, J. The frequency of planetary debris around young white dwarfs. *Astron. Astrophys.* **566**, A34 (2014).
21. Melis, C. et al. Accretion of a terrestrial-like minor planet by a white dwarf. *Astrophys. J.* **732**, 90 (2011).
22. Gänsicke, B. T. et al. The chemical diversity of exo-terrestrial planetary debris around white dwarfs. *Mon. Not. R. Astron. Soc.* **424**, 333–347 (2012).
23. Wilson, D. J. et al. The composition of a disrupted extrasolar planetesimal at SDSS J0845+2257 (Ton 345). *Mon. Not. R. Astron. Soc.* **451**, 3237–3248 (2015).
24. Buchan, A. M. et al. Planets or asteroids? A geochemical method to constrain the masses of white dwarf pollutants. *Mon. Not. R. Astron. Soc.* **510**, 3512–3530 (2022).
25. Harrison, J. H. D., Bonsor, A. & Madhusudhan, N. Polluted white dwarfs: constraints on the origin and geology of exoplanetary material. *Mon. Not. R. Astron. Soc.* **479**, 3814–3841 (2018).
26. Harrison, J. H. D. et al. Bayesian constraints on the origin and geology of exoplanetary material using a population of externally polluted white dwarfs. *Mon. Not. R. Astron. Soc.* **504**, 2853–2867 (2021).
27. Krot, A. N., Amelin, Y., Cassen, P. & Meibom, A. Young chondrules in CB chondrites from a giant impact in the early Solar System. *Nature* **436**, 989–992 (2005).
28. Jura, M., Xu, S. & Young, E. D. ^{26}Al in the early Solar System: not so unusual after all. *Astrophys. J. Lett.* **775**, L41 (2013).
29. Wasserburg, G. J., Lee, T. & Papanastassiou, D. A. correlated O And Mg isotopic anomalies in Allende inclusions: II. Magnesium. *Geophys. Res. Lett.* **4**, 299–302 (1977).
30. Tang, H. & Dauphas, N. Abundance, distribution, and origin of ^{60}Fe in the solar protoplanetary disk. *Earth Planet. Sci. Lett.* **359**, 248–263 (2012).
31. Lugaro, M., Ott, U. & Kereszturi, Á. Radioactive nuclei from cosmochronology to habitability. *Prog. Part. Nucl. Phys.* **102**, 1–47 (2018).
32. Gounelle, M. The abundance of ^{26}Al-rich planetary systems in the galaxy. *Astron. Astrophys.* **582**, A26 (2015).
33. Young, E. D. Inheritance of solar short- and long-lived radionuclides from molecular clouds and the unexceptional nature of the solar system. *Earth Planet. Sci. Lett.* **392**, 16–27 (2014).
34. Lichtenberg, T., Parker, R. J. & Meyer, M. R. Isotopic enrichment of forming planetary systems from supernova pollution. *Mon. Not. R. Astron. Soc.* **462**, 3979–3992 (2016).
35. Kuffmeier, M., Frostholm Mogensen, T., Haugbølle, T., Bizzarro, M. & Nordlund, Å. Tracking the distribution of ^{26}Al and ^{60}Fe during the early phases of star and disk evolution. *Astrophys. J.* **826**, 22 (2016).
36. Côté, B. et al. Galactic chemical evolution of radioactive isotopes. *Astrophys. J.* **878**, 156 (2019).
37. Fatuzzo, M. & Adams, F. C. Theoretical distributions of short-lived radionuclides for star formation in molecular clouds. *Astrophys. J.* **925**, 56 (2022).
38. Forbes, J. C., Alves, J. & Lin, D. N. C. A Solar System formation analogue in the Ophiuchus star-forming complex. *Nat. Astron.* **5**, 1009–1016 (2021).
39. Reiter, M. Observational constraints on the likelihood of ^{26}Al in planet-forming environments. *Astron. Astrophys.* **644**, L1 (2020).
40. Lichtenberg, T., Drążkowska, J., Schönbächler, M., Golabek, G. J. & Hands, T. O. Bifurcation of planetary building blocks during Solar System formation. *Science* **371**, 365–370 (2021).
41. Hughes, A. M., Duchêne, G. & Matthews, B. C. Debris disks: structure, composition, and variability. *Annu. Rev. Astron. Astrophys.* **56**, 541–591 (2018).
42. Marcus, R. A., Sasselov, D., Hernquist, L. & Stewart, S. T. Minimum radii of super-earths: constraints from giant impacts. *Astrophys. J. Lett.* **712**, L73–L76 (2010).
43. Carter, P. J., Leinhardt, Z. M., Elliott, T., Walter, M. J. & Stewart, S. T. Compositional evolution during rocky protoplanet accretion. *Astrophys. J.* **813**, 72 (2015).
44. Debes, J. H. & Sigurdsson, S. Are there unstable planetary systems around white dwarfs? *Astrophys. J.* **572**, 556–565 (2002).
45. Elkins-Tanton, L. T., Weiss, B. P. & Zuber, M. T. Chondrites as samples of differentiated planetesimals. *Earth Planet. Sci. Lett.* **305**, 1–10 (2011).

46. Payne, M. J., Veras, D., Holman, M. J. & Gänsicke, B. T. Liberating exomoons in white dwarf planetary systems. *Mon. Not. R. Astron. Soc.* **457**, 217–231 (2016).
47. Veras, D., Mustill, A. J., Bonsor, A. & Wyatt, M. C. Simulations of two-planet systems through all phases of stellar evolution: implications for the instability boundary and white dwarf pollution. *Mon. Not. R. Astron. Soc.* **431**, 1686–1708 (2013).
48. Veras, D. Post-main-sequence planetary system evolution. *R. Soc. Open Sci.* **3**, 150571 (2016).
49. Farihi, J. et al. Scars of intense accretion episodes at metal-rich white dwarfs. *Mon. Not. R. Astron. Soc.* **424**, 464–471 (2012).
50. Krivov, A. V. & Wyatt, M. C. Solution to the debris disc mass problem: planetesimals are born small? *Mon. Not. R. Astron. Soc.* **500**, 718–735 (2021).
51. Wyatt, M. C. Evolution of debris disks. *Annu. Rev. Astron. Astrophys.* **46**, 339–383 (2008).
52. Wyatt, M. C. et al. Steady state evolution of debris disks around a stars. *Astrophys. J.* **663**, 365–382 (2007).
53. Lichtenberg, T. & Krijt, S. System-level fractionation of carbon from disk and planetesimal processing. *Astrophys. J. Lett.* **913**, L20 (2021).
54. Wordsworth, R. & Kreidberg, L. Atmospheres of rocky exoplanets. Preprint at https://arxiv.org/abs/2112.04663 (2021).
55. Drążkowska, J., Stammler, S. M. & Birnstiel, T. How dust fragmentation may be beneficial to planetary growth by pebble accretion. *Astron. Astrophys.* **647**, A15 (2021).
56. Brewer, J. M., Fischer, D. A., Valenti, J. A. & Piskunov, N. Spectral properties of cool stars: extended abundance analysis of 1,617 planet-search stars. *Astrophys. J. Suppl. Ser.* **225**, 32 (2016).
57. Fischer, R. A. et al. High pressure metal-silicate partitioning of Ni, Co, V, Cr, Si, and O. *Geochim. Cosmochim. Acta* **167**, 177–194 (2015).
58. Corgne, A. & Wood, B. J. Element partitioning during core formation. *Geochim. Cosmochim. Acta* **72(Suppl)**, A178 (2008).
59. Wade, J. & Wood, B. J. Core formation and the oxidation state of the Earth. *Earth Planet. Sci. Lett.* **236**, 78–95 (2005).
60. Wood, B. J., Wade, J. & Kilburn, M. R. Core formation and the oxidation state of the Earth: additional constraints from Nb, V and Cr partitioning. *Geochim. Cosmochim. Acta* **72**, 1415–1426 (2008).
61. Cottrell, E., Walter, M. J. & Walker, D. Metal-silicate partitioning of tungsten at high pressure and temperature: Implications for equilibrium core formation in Earth. *Earth Planet. Sci. Lett.* **281**, 275–287 (2009).
62. Siebert, J., Badro, J., Antonangeli, D. & Ryerson, F. J. Metal-silicate partitioning of Ni and Co in a deep magma ocean. *Earth Planet. Sci. Lett.* **321**, 189–197 (2012).
63. Hollands, M. A., Koester, D., Alekseev, V., Herbert, E. L. & Gänsicke, B. T. Cool DZ white dwarfs - I. Identification and spectral analysis. *Mon. Not. R. Astron. Soc.* **467**, 4970–5000 (2017).
64. Hollands, M. A., Gänsicke, B. T. & Koester, D. Cool DZ white dwarfs II:compositions and evolution of old remnant planetary systems. *Mon. Not. R. Astron. Soc.* **477**, 93 (2018).
65. Blouin, S. Magnesium abundances in cool metal-polluted white dwarfs. *Mon. Not. R. Astron. Soc.* **496**, 1881–1890 (2020).
66. Bonsor, A. et al. Are exoplanetesimals differentiated? *Mon. Not. R. Astron. Soc.* **492**, 2683–2697 (2020).
67. Hollands, M. A., Tremblay, P.-E., Gänsicke, B. T., Koester, D. & Gentile-Fusillo, N. P. Alkali metals in white dwarf atmospheres as tracers of ancient planetary crusts. *Nat. Astron.* **5**, 451–459 (2021).
68. Zuckerman, B. et al. An aluminum/calcium-rich, iron-poor, white dwarf star: evidence for an extrasolar planetary lithosphere? *Astrophys. J.* **739**, 101 (2011).
69. Sellke, T., Bayarri, M. J. & Berger, J. O. Calibration of rho values for testing precise null hypotheses. *Am. Stat.* **55**, 62–71 (2001).
70. Xu, S. et al. Compositions of planetary debris around dusty white dwarfs. *Astron. J.* **158**, 242 (2019).
71. Wyatt, M. C., Clarke, C. J. & Booth, M. Debris disk size distributions: steady state collisional evolution with Poynting-Robertson drag and other loss processes. *Celest. Mech. Dynam. Astron.* **111**, 1–28 (2011).
72. Dohnanyi, J. S. Collisional model of asteroids and their debris. *J. Geophys. Res.* **74**, 2531–+ (1969).
73. Benz, W. & Asphaug, E. Catastrophic disruptions revisited. *Icarus* **142**, 5–20 (1999).
74. Durda, D. D., Greenberg, R. & Jedicke, R. Collisional models and scaling laws: a new interpretation of the shape of the main-belt asteroid size distribution. *Icarus* **135**, 431–440 (1998).
75. Löhne, T., Krivov, A. V. & Rodmann, J. Long-term collisional evolution of debris disks. *Astrophys. J.* **673**, 1123–1137 (2008).
76. Wyatt, M. C. et al. Transience of hot dust around Sun-like stars. *Astrophys. J.* **658**, 569–583 (2007).
77. Bonsor, A. & Wyatt, M. Post-main-sequence evolution of a star debris discs. *Mon. Not. R. Astron. Soc.* **409**, 1631–1646 (2010).

Acknowledgements

A.B. acknowledges support from a Royal Society Dorothy Hodgkin Research Fellowship (grant number DH150130) and a Royal Society University Research Fellowship (grant number URF\R1\211421). T.L. was supported by a grant from the Simons Foundation (SCOL award number 611576). J.D. acknowledges funding from the European Research Council (ERC) under the European Union's Horizon 2020 research and innovation programme under grant agreement number 714769. A.M.B. acknowledges support from a Royal Society funded PhD studentship (grant number RGFEA180174). We acknowledge fruitful discussions with M. Brouwers, L. Rogers, E. Lynch, A. Curry, T. Birnstiel, M. Wyatt and R. J. Parker.

Author contributions

The idea for the study came from discussions between A.B., J.D. and T.L. The analysis of the white dwarf data was performed by A.M.B. and T.L. supplied the thermal evolution models used for Fig. 2. All authors contributed to writing the manuscript.

Competing interests

The authors declare no competing interests.

Additional information

Supplementary information The online version contains supplementary material available at https://doi.org/10.1038/s41550-022-01815-8.

Correspondence and requests for materials should be addressed to Amy Bonsor.

Peer review information *Nature Astronomy* thanks the anonymous reviewers for their contribution to the peer review of this work